Characterization of three-dimensional structure using images

Bin Liu, J. Goree, and W. D. Suranga Ruhunusiri
Department of Physics and Astronomy, The University of Iowa, Iowa City, Iowa 52242, USA

(Received 23 January 2015; accepted 19 February 2015; published online 17 March 2015)

The pair correlation function $g(r)$ and the number density n for particles in a three-dimensional (3D) sample can be determined from a single two-dimensional (2D) image. The 2D image is obtained experimentally with a simple setup: a cross-sectional slab of particles is illuminated with a laser sheet and imaged with a single camera. After image analysis, to find positions of particles in two dimensions, along with their brightness, one obtains $g(r)$, also known as the radial distribution function. The key for attaining high accuracy is to use only the particles that are brighter than a filter level, which we refine to achieve greater accuracy. The density n is obtained from $g(r)$. This method is demonstrated in a dusty plasma experiment. Accuracy is quantified using simulation data; errors of 2% for both the pair correlation function and the number density are achievable. The method is useful for dusty plasmas and colloids. © *2015 AIP Publishing LLC.* [http://dx.doi.org/10.1063/1.4914468]

I. INTRODUCTION

Number density n and the pair correlation function $g(r)$ are widely used to characterize the structural arrangement of particles such as molecules in liquids and microspheres in colloidal suspensions[1,2] or dusty plasmas.[3–5] The correlation function $g(r)$ expresses the probability of finding a particle at a distance r from another particle.[6] Quantification of n and $g(r)$ are often needed in both theory and experiments. Here, we are mainly interested in systems, where the particles fill a 3D volume but are viewed experimentally with only two dimensional images. We will use subscripts 2 or 3 to distinguish $g_2(r)$ obtained using a two-dimensional image and $g_3(r)$ for the true pair correlation function of a 3D sample. The true three-dimensional number density is denoted n_3.

The standard calculation of $g(r)$ can be done for either two-dimensional (2D) or 3D systems. For a two-dimensional system, the calculation of $g_2(r)$ requires as its input the (x, y) coordinates of each particle. One counts the number of particles in an annular ring centered on one central particle and divides by the area $2\pi r dr$ between radii r and $r + dr$. Repeating for all such central particles in the region of interest and averaging, one obtains $g_2(r)$ for one value of r. This is repeated for many values of r to generate a graph of $g_2(r)$. For a three-dimensional system, the standard calculation of $g_3(r)$ is similar, except that r is now a radius in three dimensions; an annular spherical shell of volume $4\pi r^2 dr$ is used instead of an annular ring when counting particles; the calculation of $g_3(r)$ requires as its input the (x, y, z) coordinates of all particles.

In this paper, we demonstrate that n_3 and $g_3(r)$ for a three-dimensional sample can be determined with surprising accuracy using only the two-dimensional (x, y) coordinates along with the brightness of each particle. The advantage of doing so is that the instrumentation is simplified; one can use a common 2D imaging configuration.[7] For micron-size particles, such a two-dimensional imaging configuration is sketched in Fig. 1(a) with a single camera. The depth of the volume that is imaged is determined either by the camera lens depth-of-focus or by the thickness of an illumination laser sheet.[8] If the particles are widely spaced, i.e., if their volume fraction is small, they can be illuminated by a planar sheet of light, and the camera views this sheet at 90°. The laser sheet has a finite thickness, with an intensity that must vary gradually with distance from the midplane of the laser sheet. It is obvious that this configuration for imaging particles will work well for samples with particles that lie only in a single plane (2D systems), and indeed it is widely used for that purpose with 2D colloidal suspensions,[9,10] 2D dusty plasmas,[11–14] and 2D granular media.[15]

Here, we are interested in using this simple 2D imaging configuration to measure particles filling a three-dimensional (3D) volume. A theory[16] predicts that $g_3(r)$ in a 3D homogeneous and isotropic system can be reproduced from 2D observations of a thin slab of particles. This idea has also occurred to previous experimenters who have reported $g_3(r)$ determined with such a setup from two-dimensional images recorded in a 3D dusty plasma.[17–19] These experimenters, however, did not specify the details of their image analysis method, and the accuracy of the $g_3(r)$ depends on the choice of particles included in the calculation, as we will show in this paper. In this paper, we specify an experimental method in detail, demonstrate its use, and find its accuracy for determining $g_3(r)$ and n_3 using a common 2D imaging setup.

The problem with using a 2D image to obtain the 3D number density n_3 is that there is seemingly no unique answer. This can be seen by comparing the images in Figs. 1(b) and 1(c), which were recorded experimentally for the same sample of dusty plasma but a different width for the illuminating laser sheet. The experiment is described in Sec. III. In these images, more particles are visible if the laser sheet is thicker. If one simply counts the number of particles that are visible and divides the number by a volume, the result is unreliable because the volume is not well defined because of a brightness that diminishes gradually in the out-of-plane direction. Similarly, there is apparently no unique answer for $g_3(r)$, based on such an image.

In this paper, we present a method that overcomes this problem by exploiting the variation of brightness of particles

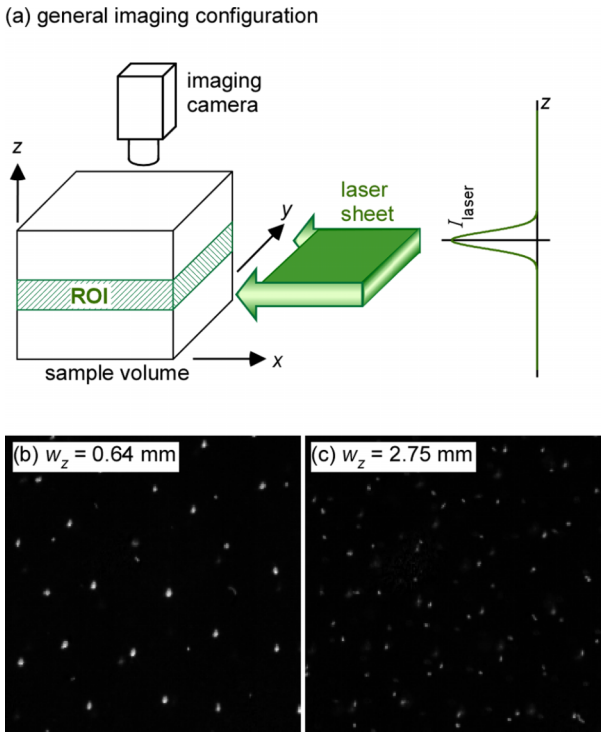

FIG. 1. (a) Two-dimensional imaging configuration. Experimental images, from the same experiment, of a slab of particles in a dusty plasma as illuminated by a laser sheet of Gaussian half-width (b) $w_z = 0.64$ mm and (c) $w_z = 2.75$ mm. Note that the spot brightnesses vary from one particle to another. More particles are visible in the image in (c), due to a thicker laser sheet.

according to their position within the laser sheet.[20] This brightness variation can be seen in the images in Figs. 1(b) and 1(c). In our method, we filter the particles according to their brightness to determine which will be included in the calculations. (In general, one could weight the particles according to their intensities; our filtering step uses a weighting function that is a simple step function.) After filtering, we first obtain $g_2(r)$ with a two-step determination, where the second step is a refinement of the first. Thusly, obtained $g_2(r)$ is a reasonable experimental representation of $g_3(r)$. Finally, from this representation of $g_3(r)$, we compute the three-dimensional number density n_3. In principle, this method can be used with a single two-dimensional image, so that the experimenter can obtain time-resolved measurements of $g_3(r)$ and n_3.

There are several other imaging methods that can yield $g_3(r)$ and n_3 in a 3D sample. They all require a more elaborate instrumentation than the simple 2D setup we consider. One approach is to scan the position of both the laser sheet and the camera so that over time all the particles in the sample volume are imaged.[21] The data so obtained are not simultaneous, meaning that this method is best used when particles move very slowly. For sample volumes with small numbers of particles, either stereoscopic imaging with three cameras[22] or digital holography[23,24] with a single camera allows recording the simultaneous determination of positions of particles in 3D. In confocal imaging, as used in colloidal suspensions, a laser beam is rastered and a stack of 2D image slices is collected by progressively stepping the focal plane of the objective through a sample to construct images within a 3D volume.[2] These methods yield the 3D positions of individual particles, while the method we report does not. Our method yields $g_3(r)$ and n_3 without providing more detailed 3D description of individual particles, but it has the advantage of simplicity in its imaging instrumentation.

II. ANALYSIS METHOD

A. Overview

The input for the method is a single two-dimensional gray-scale image. Portions of such an image are shown in Figs. 1(b) and 1(c). Starting with such an image, our method has the following sequence:

- Preprocess the image.
- Make a two-step determination of $g_2(r)$ as a representation of $g_3(r)$.
- Find n_3 using the $g_3(r)$ data.

B. Preprocessing

In a 2D gray-scale image, a particle generally fills multiple pixels. The brightness of a particle will vary depending on its position within the nonuniform intensity profile of the laser sheet. Portions of such images are shown in Figs. 1(b) and 1(c). A digital image is essentially a 2D array of integers I_{ij}, where I represents the brightness within one pixel with a position (i, j) in the image.

We preprocess a 2D image to obtain a list of particles appearing in the image to yield three values for each particle: its x and y positions and its intensity. Several standard methods in the literature allow a determination of the x and y positions with sub-pixel resolution. Any of these methods could be used; the subsequent filtering step needs only the x and y positions and intensities, and it is not crucial how these quantities are obtained. For the purpose of the demonstration in Sec. III, we will choose the moment method[26] to obtain the x and y positions. (In the moment method, the central position of a bright spot is determined as a weighted average of pixel positions i and j, where the weighting is proportional to the intensities I_{ij} and pixels that are included are selected by a thresholding scheme. The sub-pixel accuracy of the moment method is improved by subtracting a background image and making a careful choice of the threshold level.)

In addition to the x and y positions of each particle, we will also require its brightness. One can determine the brightness most simply as the largest value I_{ij} of all the pixels within the particle's image, and we will find this simple method provides adequate accuracy in our simulation test of Sec. V. Alternatively, with slightly greater effort, one could characterize the brightness of a particle by summing the intensities of all pixels I_{ij} within its image; this would reduce sensitivity to noise in a pixel.

C. Filter level

To obtain the three-dimensional $g_3(r)$ using the (x, y) coordinates and brightness of particles instead of using the

(x, y, z) coordinates, we will devote most of our attention to the use of the brightness data. In particular, we will select the particles that are included in the calculation of $g_2(r)$ according to whether they are brighter than a "filter level." Only particles brighter than the filter level will be included in the determination of $g_2(r)$. By choosing this filter level appropriately, the $g_2(r)$ so obtained will closely match the true $g_3(r)$.

The "filter level" is a particular choice of a minimum brightness I_{min}. If the particles are all identical, all the particles brighter than I_{min} lie within a slab inside the laser sheet. Thus, a lower filter level means that a thicker slab is analyzed. The requirement in choosing a filter level is essentially a compromise, to make the slab neither too thick nor too thin, so that the so obtained $g_2(r)$ will match $g_3(r)$.

Selecting the filter level is the key to obtaining an accurate graph of the three-dimensional $g_3(r)$ using a two-dimensional image. We will present two schemes of selecting the filter level, yielding two different determinations of $g_3(r)$. Both schemes use a graph of the number of particles that are brighter than the minimum brightness I_{min}, as shown in Fig. 3. This graph has a monotonic downward trend, meaning that if one chooses a larger value of I_{min}, fewer particles will be counted. This is so because the laser sheet's illumination becomes gradually less intense with greater distance from the midplane of the sheet. This graph is our only use of the brightness data for particles.

The two schemes that we choose the filter level are presented in Secs. II D and II E. In the first determination of $g_2(r)$, we choose a filter level graphically by examining asymptotes in the particle-number graph. In the second determination, the filter level is chosen differently, with two inputs: the $g_2(r)$ data from the first determination and the particle-number graph. The user could use only our first determination of $g_2(r)$, but the second one can be valuable in two ways: the $g_2(r)$ obtained this way is a more accurate representation of the true $g_3(r)$ (according to our test with synthetic data), and one can estimate the errors in the determination of $g_3(r)$ by comparing the two determinations.

D. First determination of $g_2(r)$ as a representation of $g_3(r)$

Before determining n_3, we generate $g_2(r)$. In our first determination of $g_2(r)$, we choose a filter level using a scheme based on the variation trends in the particle-number graph. We identify two asymptotes in the graph, and the filter level is chosen as the value of I_{min} where the two asymptotes intersect. This scheme is simple to use, and as its input, it only requires the particle-number graph. Using the filter level from this scheme to choose the particles in the image, one then uses the standard two-dimensional method of calculating $g_2(r)$ by counting particles in annular rings, as introduced in Sec. I.

E. Second determination of $g_2(r)$ as a representation of $g_3(r)$

The second determination of $g_2(r)$ uses a different filter level. To choose this filter level, we first examine the graph of $g_2(r)$ from the first determination to find the radius r_{nn} of the largest peak. We next calculate a number of particles

$$N_f = CAr_{nn}^{-2}, \tag{1}$$

where A is the area of the analyzed region in the two-dimensional image. The dimensionless coefficient C has a typical value of 0.43, as we explain below. Finally, we examine the particle-number graph, such as Fig. 3, and find the value of I_{min} on its horizontal axis that corresponds to N_f on the vertical axis.

The dimensionless coefficient C in Eq. (1) determines how thick the slab will be. In this paper, we use $C = 0.43$, which we determined empirically in the simulation described in the Appendix for a slab of thickness $\sqrt{3}r_{nn}/4$. We will find in Sec. V that using this value for C, one can obtain $g_3(r)$ with errors as small as 2%.

After selecting the filter level using Eq. (1), we again compute $g_2(r)$ using the standard method (as described in the Sec. I), including in the calculation only those particles that are brighter than the filter level.

F. Determination of the number density

After obtaining $g_2(r)$ as a representation of $g_3(r)$, and in particular the radius r_{nn} of its largest peak, we can determine the three-dimensional number density. The expression to use for this purpose is

$$n_3 = \frac{3}{4\pi}\frac{\rho^3}{r_{nn}^3}, \tag{2}$$

where $\rho \equiv r_{nn}/a_{WS}$ is a dimensionless ratio of r_{nn} and the Wigner-Seitz radius a_{WS}. The Wigner-Seitz radius in three-dimensions is defined by

$$n_3 = \frac{3}{4\pi a_{WS}^3}. \tag{3}$$

The value of the ratio ρ will depend slightly on the interaction potential. For a Yukawa potential, we empirically find $\rho = 1.79 \pm 0.07$ using simulation data, as described in the Appendix. The ± 0.07 variation corresponds to a $\pm 4\%$ systematic error; it arises from sensitivity to thermodynamic parameters. The $\pm 4\%$ uncertainty in ρ will correspondingly cause an uncertainty of $\pm 12\%$ in the number density obtained using Eq. (2).

Equations (2) and (3) are intended only for isotropic liquids. For an anisotropic system, such as a dusty plasma in the presence of flowing ions, the method of this paper can still be used to calculate $g_3(r)$ and n_3. However, the results might not precisely describe the position of particles in all three directions since $g_3(r)$ with a scalar r cannot be an adequate structural measure for an anisotropic system.

III. DEMONSTRATION EXPERIMENT

We demonstrate the method in Sec. II using an experiment with a dusty plasma, which is a collection of micron-size particles of solid matter immersed in a partially ionized gas-discharge plasma. Depending on the conditions, the particles

can arrange themselves into a structure like that of molecules in a liquid or crystal.

The setup of our demonstration experiment is shown in Figs. 1(a) and 2. A radio-frequency (RF) discharge plasma is made using Ar gas at a pressure of 200 mTorr and 13 MHz RF power with a peak-to-peak amplitude of 114 V. Melamine-formaldehyde polymer microsphere particles of 4.8 μm diameter are levitated and confined by electric fields, which are shaped by a glass box. The particles self-organize. Their positions resemble the arrangement of molecules in a 3D liquid. A slab of the particles is illuminated by a horizontal sheet of 576 nm laser light, which has a Gaussian intensity profile in the vertical z direction. Particles so illuminated are viewed from above with a 12-bit camera at 50 frames/s, with a resolution of 12.9 μm per pixel. Bit mapped images, recorded as 16-bit files, are produced for each video frame. For further details of the experimental setup, see Ref. 25.

IV. ILLUSTRATION OF METHOD WITH EXPERIMENTAL DATA

We next present further details of the analysis method in Sec. II, illustrating them using data from the experiment.

A. Particle-number graph

The key to obtain accurate determination of $g_3(r)$ and n_3 is the choice of a filter level. The main tool for choosing the filter level is a graph of the number of particles that are brighter than an adjustable level $I_{\min}$, Fig. 3. This graph is prepared after the 2D images are preprocessed to yield particle coordinates (x, y) and pixel intensity I_{ij}. For our demonstration experiment, this preprocessing identified 279 particles in a single image. (The filtering schemes described below will select some of the brightest of these 279 particles.) From the preprocessed data for this single image, we count the number of particles that has at least one pixel brighter than $I_{\min}$, and we plot that count vs. $I_{\min}$, yielding Fig. 3. We will refer to this as "the particle-number graph."

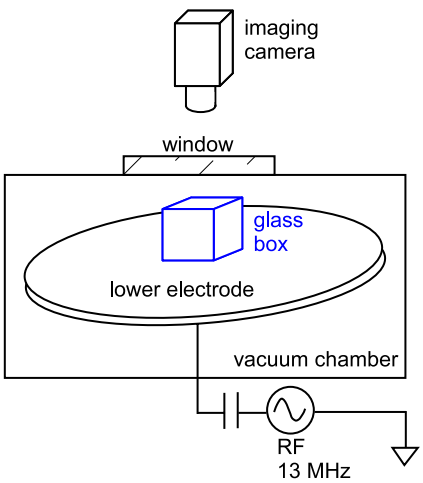

FIG. 2. Dusty plasma experiment setup. The illumination scheme is sketched in Fig. 1(a).

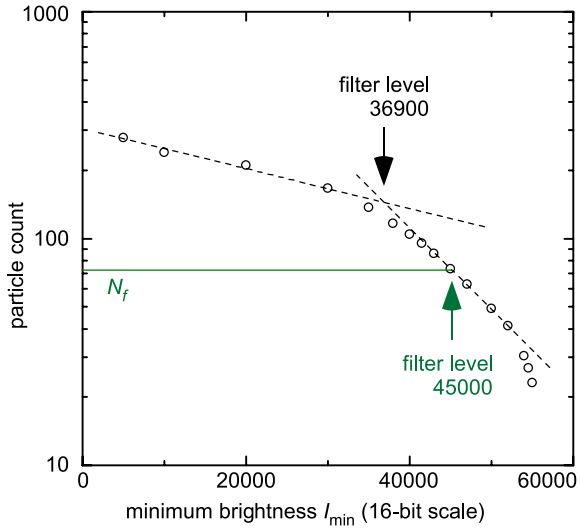

FIG. 3. Particle-number graph. The intersection of asymptotes in this graph provides the filter level for the first determination of $g_2(r)$; in this case, the resulting filter level is a pixel brightness of 36 900. Also shown is the filter level for the second determination of $g_2(r)$, which in this case is 45 000. Data are from the experiment, using a laser sheet width of $w_z = 0.64$ mm, as in Fig. 1(b).

The particle count in Fig. 3 decreases monotonically with increasing $I_{\min}$. This trend is expected for an illumination laser sheet that becomes less bright with greater distance z from the laser sheet's midplane. More particles near the edge of the illumination laser sheet are eliminated in our filtering process as $I_{\min}$ is increased. A higher filter level is equivalent to reducing the slab width (in the z direction) of the particles to be sampled.

B. First determination of $g_2(r)$

Our determination of $g_2(r)$ as a representation of $g_3(r)$ relies on selecting particles according to their brightness using a filter level. In our first determination, we choose a filter level as the intersection of the asymptotes in the particle-number graph, as shown in Fig. 3. For our experiment, we find that two asymptotes intersect at $I_{\min} = 36\,900$, as indicated by the two dashed lines in Fig. 3. In the case of our experiment, this filter level selects only 129 of the 279 originally identified particles. Calculating $g_2(r)$ using the standard two-dimensional method, for these 129 particles, yields the curve marked as scheme 1 in Fig. 4. A feature of interest in this graph is the radius r_{nn} of the first peak of $g_2(r)$.

C. Second determination of $g_2(r)$

Our second determination of $g_2(r)$ relies on selecting particles in a slab that has a thickness different from the first determination. This is done by finding a different filter level in two steps. First, we use the first determination of $g_2(r)$ to estimate the radius r_{nn} of its largest peak, yielding $r_{nn} = 0.51$ mm for our experiment, as seen in Fig. 4. We then use Eq. (1) to calculate N_f, which for our experiment is $N_f = 76$. Second, using the particle-number graph Fig. 3, we find that the number

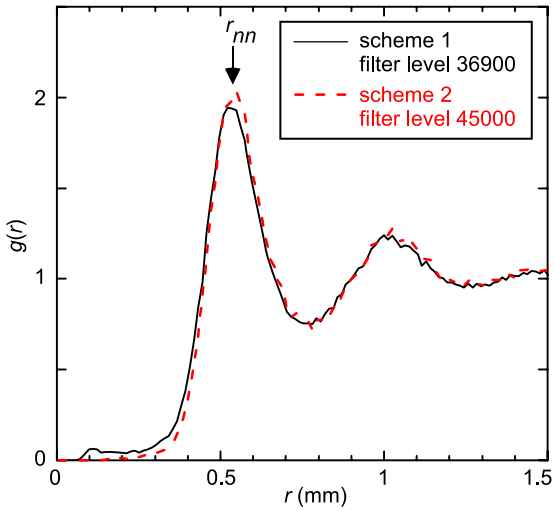

FIG. 4. Pair correlation functions determined from experimental images. Results marked as schemes 1 and 2 are from our two determinations, using different filter levels.

$N_f = 76$ corresponds to $I_{min} = 45\,000$, which is our filter level for the second determination.

Again using the standard calculation method for $g_2(r)$, we obtain our second determination of $g_2(r)$. For our experiment, the result is also shown in Fig. 4, marked as scheme 2. We can also now refine our estimate of r_{nn} by fitting four data points in the first peak of $g_2(r)$ to a parabola, yielding $r_{nn} = 0.543$ mm.

D. Determination of number density

The number density n_3 is determined using Eq. (2) using the radius r_{nn} of the largest peak of $g_2(r)$. Using $r_{nn} = 0.543$ mm in Eq. (2) with $\rho = 1.79$ yields our result for n_3, which is 8.552 mm^{-3}. As discussed earlier, this measurement could have an error of 12%, arising from the uncertainty in ρ.

V. ACCURACY OF METHOD

The accuracy of our analysis method is evaluated using data from a simulation. The advantage of a simulation, as compared to an experiment, is that the true particle positions are known, so that the true $g_3(r)$ and n_3 are also known. We generate synthetic images that are based on the true positions and then perform the same analysis method starting with these synthetic images exactly as we would with experiment images. Comparing to the known values yields the measurement errors for $g_3(r)$ and n_3.

A. Simulation

We use a Langevin molecular dynamics simulation to generate true particle positions (x, y, z) and the corresponding true values for $g_3(r)$ and n_3. This simulation mimics a 3D volume of micron-size particles in a dusty plasma, tracking individual particles by integrating the equation of motion for each one. We confine $N = 12\,800$ particles within a rectangular volume of $132.0 \times 81.0 \times 79.4\ \lambda_D{}^3$, corresponding to Wigner-Seitz radius $a_{WS} = 2.4\lambda_D$. The screening length λ_D is a dusty plasma parameter explained in the Appendix; for the simulation, in this paper, we chose $\lambda_D = 0.083$ mm, which is typical for experiments. Figure 5(a) shows example results for the simulated particle positions, with a 3D structural arrangement that is typical of isotropic liquids. For further details of the simulation, see the Appendix.

To assess the accuracy of our analysis method, we use the method of Ref. 26 to generate synthetic images. Each particle is assigned a brightness and is projected onto a 2D plane. The laser illumination is assumed to have a Gaussian intensity profile in the z direction, with a half-width $w_z = 150\ \mu$m. In converting the brightness into pixel intensity, we integrate the Gaussian intensity profile over each pixel's area. After integrating the intensity within a square pixel, a random error is introduced into the intensity of that pixel.[27] Figure 5(a) is a snapshot in three dimensions, of the true particle positions, with a darker color representing a brighter illumination. Figure 5(b) is a projection of these particles onto the x–y plane. Assuming an 8-bit camera, as, for example, in the PK-4 experiment on the International Space Station,[29–31] the pixel brightness ranges from 0 to 255. The simulation mimics experimental conditions, where an experimenter has followed

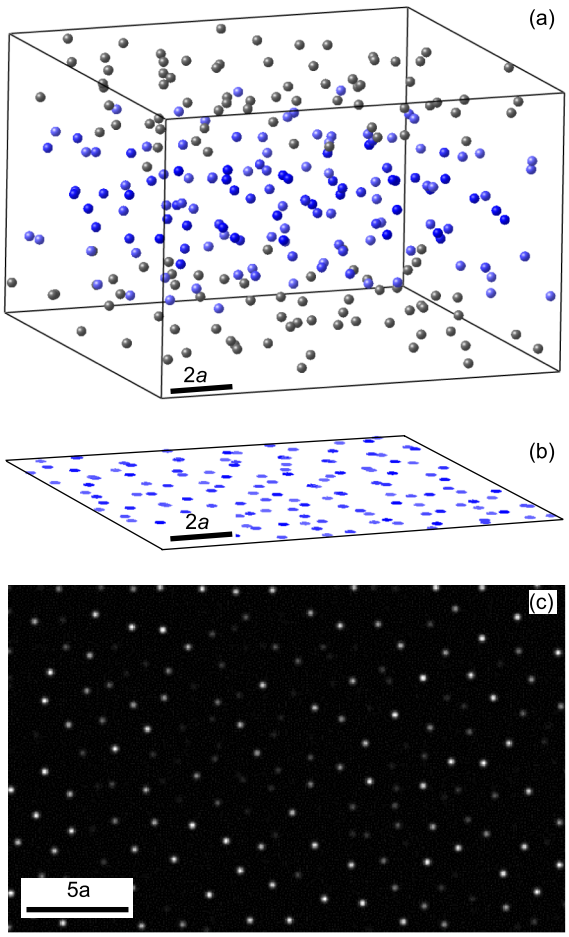

FIG. 5. True positions for the simulation in 3D (a), and their 2D projections onto the x–y plane (b). A darker color indicates greater laser illumination. A synthetic 8-bit monochrome bit-map image (c) is produced from the projection. A computer file for this image can be downloaded from the supplementary material.[28]

the recommendation of Ref. 26 to adjust the camera exposure so that just a few pixels in the image are saturated (at a level of 255). In the PK-4 experiment, the camera resolution is 13.9 μm per pixel. Projecting the simulation volume onto the $x-y$ plane yields a 788×489 pixel monochrome bit-map image shown in Fig. 5(c). This is the synthetic image we test for errors.

B. $g_3(r)$ and its error

We determine $g_3(r)$ from the synthetic images using the same analysis method as in Sec. II. The synthetic images are first preprocessed, yielding identified particles with their coordinates and brightness data. We then prepare a particle-number graph, Fig. 6.

For the first determination, we choose a filter level as the intersection of two asymptotes, shown in Fig. 6. In this example, the two asymptotes intersect as indicated by the two dashed lines so that $I_{min} = 235$ is chosen as our first filter level. We then use the standard 2D method to compute $g_2(r)$ including only the 98 particles that are brighter than this filter level. The result for $g_2(r)$ is shown as symbols in Fig. 7(b). For comparison, we also show the true $g_3(r)$ as a smooth curve. We see that even for this first determination, our method is already achieving reasonable accuracy; the symbols in Fig. 7(b) almost match the smooth true curve.

Also shown in Fig. 7(a), to demonstrate the importance of the filter level, is a pair correlation function computed with no filtering. We see that $g_2(r)$ determined with unfiltered particles has much larger errors than when filtering is used.

Our second determination of $g_2(r)$ is shown as symbols in Fig. 7(c). This result is calculated using 265 particles instead of 98, as selected by our second filter level 174. (To choose the second filter level we used the measurement $r_{nn} = 4.2\,\lambda_D$ from $g_2(r)$ in Fig. 7(b) to yield a desired number of particles $N_f = 265$ as shown in Fig. 6, corresponding to a filter level of 174.) Comparing to the true $g_3(r)$, we see that the second determination of the pair correlation function from Fig. 7(c) has been refined, so that the agreement with the true $g_3(r)$ is quite good.

To continue our test, we seek a single number that quantifies how closely the determined $g_2(r)$ matches the true

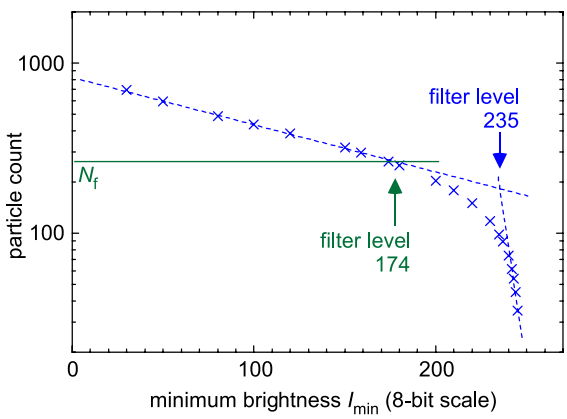

FIG. 6. Particle-number graph from synthetic images. Two filtering levels are chosen using the same two schemes as for demonstration experiment.

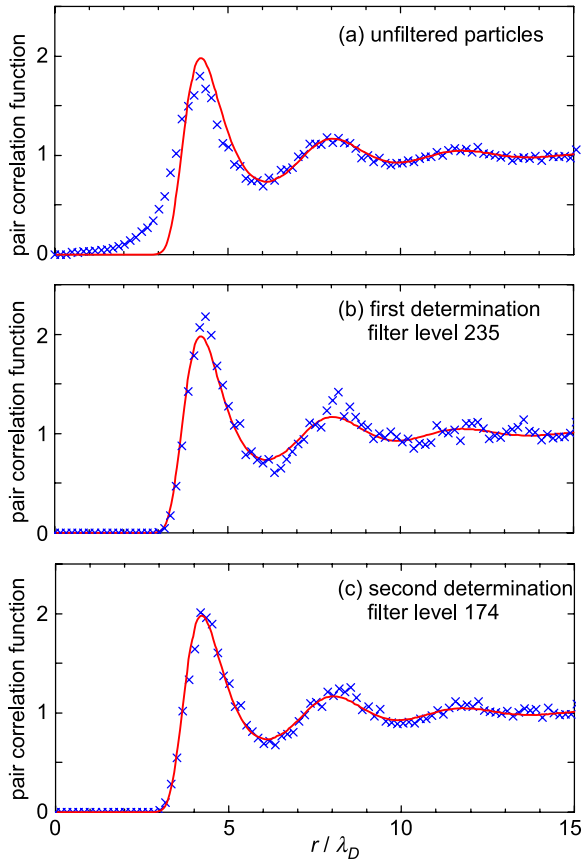

FIG. 7. Comparison of pair correlation functions: 3D accurate (smooth curves) and 2D measurements (symbols). The result in (a) is calculated using unfiltered particles. Results determined using our method with filtered particles: (b) first determination with a filter level of 235 and (c) second determination with a filter level of 174. We expect that for most applications, the refinement provided by the second determination is sufficient.

$g_3(r)$. We do this two ways. First, we calculate a fractional root-mean-square (rms) error

$$\frac{\sqrt{\int_0^{1.5r_{nn}} [g_2(r) - g_3(r)]^2 dr}}{\int_0^{1.5r_{nn}} g_3(r) dr}. \tag{4}$$

The integration limits correspond to the first minimum in the pair correlation function. The data for Eq. (4) are discretized in position, so that the integrals in Eq. (4) are computed numerically, using Origin graphics software. The result for the fractional rms error, calculated for our synthetic image, is 6.3% and 4.6% for the first and second determinations of $g_2(r)$, respectively.

Second, we evaluate an error using only the first peak in the pair correlation function. As seen from Figs. 7(b) and 7(c), the first peaks are taller than that for the true $g_3(r)$. The error is 10% and 2% for the first and second determinations, respectively.

C. Number density and its error

As in the experiment, we obtain the number density using Eq. (2). We use a measurement $r_{nn} = 4.32\lambda_D$ from the first peak of $g_2(r)$ in Fig. 7(c). The number density is then

calculated to be $n_3 = 0.0170\lambda_D{}^{-3}$. The true number density is $n_3 = 0.0173\lambda_D{}^{-3}$, so that the error of our determined number density is about 2%. As discussed earlier, in general, n_3 determined by our method could have an uncertainty of as much as 12%, due to the unknown value of ρ for an experiment.

VI. CONCLUSION

We demonstrated that n_3 and $g_3(r)$ for a three-dimensional sample can be obtained with good accuracy using only the (x, y) coordinates and the brightness of each particle. This determination requires a 2D image of a slab of particles in a 3D volume. The advantage of this approach is that it can be done using a simple imaging setup with a single camera.

Our method to determine $g_3(r)$ and n_3 was demonstrated experimentally using a 3D volume of micron-size particles immersed in a glow-discharge plasma.

The pair correlation function is determined first, in two steps with slightly different filter levels. The second filter level is a refinement based on the first determination. The number density is then obtained from the first peak of $g_3(r)$.

We tested the accuracy using simulation data, with known true positions to generate synthetic images that resemble those in dusty plasma experiments. We found that we can achieve errors as small as 2% for both $g_3(r)$ and n_3.

The choice of a filter level has a significant impact on the accuracy. The main result of this paper is that there is a method of choosing the filter level to achieve good accuracy.

ACKNOWLEDGMENTS

We thank M. Thoma for information on the PK-4 camera. This work was supported by NASA and NSF.

APPENDIX: SIMULATION

Here, we present the details of our Langevin molecular dynamics simulation.

1. Method

We use a Langevin molecular dynamics simulation. We integrate each particle's equation of motion, which includes the gas drag force, a fluctuating force corresponding to the kinetic temperature T_p, particle-particle interaction due to a Yukawa repulsion, and the electric force due to electrostatic confinement. Here, we present a summary of the simulation method; further details can be found in Ref. 32.

The physical system we simulate is described by two dimensionless parameters. The Coulomb coupling parameter is defined as

$$\Gamma = \frac{Q^2}{4\pi\varepsilon_0 a_{WS} k_B T_p},$$

where Q is particle charge. The screening parameter is

$$\kappa = \frac{a_{WS}}{\lambda_D},$$

where λ_D is a screening length. In this paper, the screening length is $\lambda_D = 0.083$ mm. In a dusty plasma, the screening length λ_D is due to the ambient ions and electrons that fill the space between the micron-size charged particles.

Our simulation includes $N = 12\,800$ particles confined in a rectangular volume. To vary κ, we use different sizes for the simulation volume. For $\kappa = 2.4$, the size is $131 \times 81 \times 69\ \lambda_D^3$. The other values used in our simulation are $\kappa = 1.4$ and 4. The results presented in the paper are mainly for $\kappa = 2.4$; the other values for κ were used in tests to generate empirical values for the ratio ρ and the coefficient C of Eq. (1).

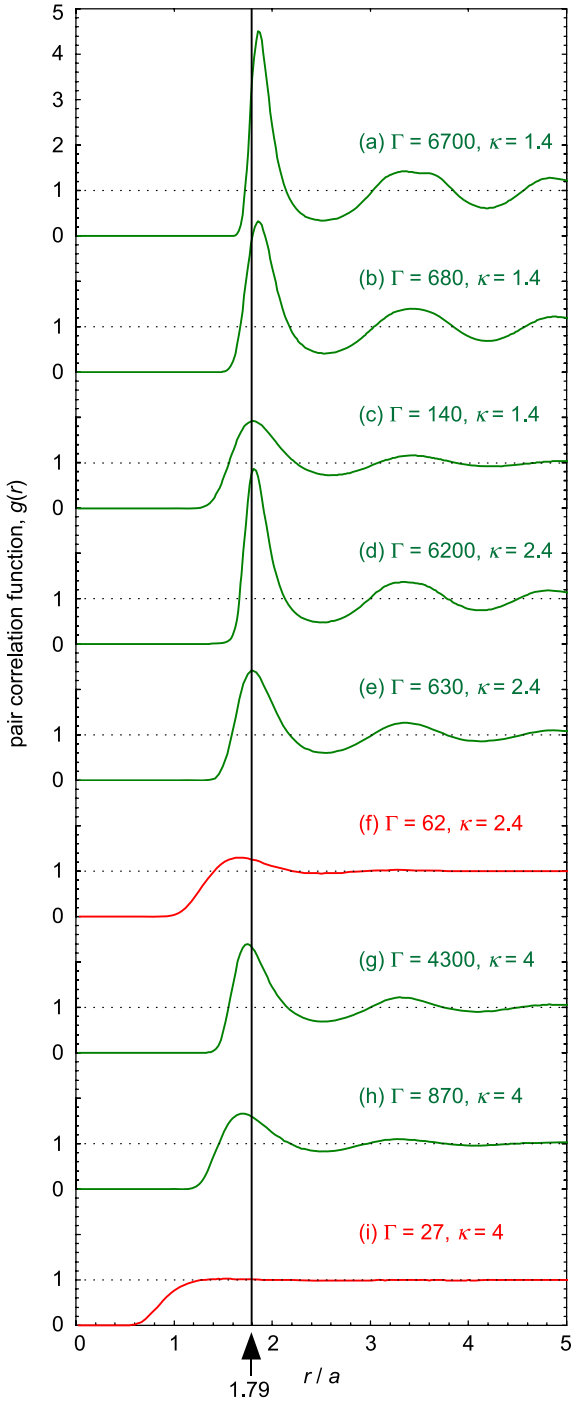

FIG. 8. Pair correlation function, $g(r)$, for 3D Yukawa system, using parameters typical for dusty plasmas. The first peak position is located near $r_{nn}/a \approx 1.79$, for curves all that have a first peak height of $g_{max} > 1.3$.

Our simulation covers a wide range of system states. We vary T_p, with a coupling parameter in the range of $27 < \Gamma < 10^5$. This range includes system states from non-ideal gases to cold liquids. Figure 5(a) in Sec. V shows a structural arrangement of a cold liquid for $\Gamma = 312$ and $\kappa = 2.4$.

2. Pair correlation function $g(r)$ for 3D dusty plasma

Figure 8 shows examples of the 3D pair correlation function $g_3(r)$, for a wide range of Γ and κ. These were calculated from snapshots of the 3D particle positions from our MD simulation data. For the parameters we simulate, the height g_{max} of the first peak of $g_3(r)$ is in a range of 1 to 4.5, corresponding to system states from non-ideal gases to cold liquids.

We find that the first peak of $g_3(r)$ is centered at r_{nn}/a_{WS} that is typically in a range between 1.4 for a hot liquid and 1.9 for a cold liquid near freezing point, depending on Γ and κ. Averaging all the data having $g_{max} > 1.3$, we find an empirical value

$$\rho \equiv r_{nn}/a_{WS} = 1.79 \pm 0.07,$$

where the $\pm$ uncertainty is due to the range of values that depend on Γ and κ. For a non-ideal gas with $g_{max} < 1.3$, the ratio ρ should be chosen in the range 1.3–1.4.

[1]K. H. Lin, J. C. Crocker, V. Prasad, A. Schofield, D. A. Weitz, T. C. Lubensky, and A. G. Yodh, Phys. Rev. Lett. **85**, 1770 (2000).
[2]P. Varadan and M. J. Solomon, J. Rheol. **47**, 943 (2003).
[3]J. H. Chu and I. Lin, Phys. Rev. Lett. **72**, 4009 (1994).
[4]A. Melzer, A. Homann, and A. Piel, Phys. Rev. E **53**, 2757 (1996).
[5]R. A. Quinn, C. Cui, J. Goree, J. B. Pieper, H. Thomas, and G. E. Morfill, Phys. Rev. E **53**, R2049 (1996).
[6]N. H. March and M. P. Tosi, *Introduction to Liquid State Physics* (World Scientific, Singapore, 2002), Chap. 4.
[7]W. D. Suranga Ruhunusiri and J. Goree, IEEE Trans. Plasma Sci. **42**, 2688 (2014).
[8]In an experiment, the laser sheet may be thinner or thicker than the depth-of-field of a camera lens. We have only tested the case where it is thinner, in our tests of computing $g(r)$ and n using simulation data. In the opposite case, the particles might not appear to be Gaussian in their shape, so that the synthetic images we used in our test would not be applicable. We anticipate that our method could also work for the case of a thicker laser sheet, but the quantitative criteria for choosing a filter level might be different.
[9]C. A. Murray and R. A. Wenk, Phys. Rev. Lett. **62**, 1643 (1989).
[10]D. G. Grier and C. A. Murray, J. Chem. Phys. **100**, 9088 (1994).
[11]U. Konopka, L. Ratke, and H. M. Thomas, Phys. Rev. Lett. **79**, 1269 (1997).
[12]S. Nunomura, J. Goree, S. Hu, X. Wang, and A. Bhattacharjee, Phys. Rev. E **65**, 066402 (2002).
[13]C. A. Knapek, D. Samsonov, S. Zhdanov, U. Konopka, and G. E. Morfill, Phys. Rev. Lett. **98**, 015004 (2007).
[14]T. E. Sheridan, Phys. Plasmas **15**, 103702 (2008).
[15]P. M. Reis, R. A. Ingale, and M. D. Shattuck, Phys. Rev. Lett. **96**, 258001 (2006).
[16]H. Totsuji, J. Phys. Soc. Jpn. **79**, 064002 (2010).
[17]V. E. Fortov, O. S. Vaulina, O. F. Petrov, V. I. Molotkov, A. M. Lipaev, V. M. Torchinsky, H. M. Thomas, G. E. Morfill, S. A. Khrapak, Y. P. Semenov, A. I. Ivanov, S. K. Krikalev, A. Yu Kalery, S. V. Zaletin, and Yu. P. Gidzenko, Phys. Rev. Lett. **90**, 245005 (2003).
[18]T. S. Ramazanov, K. N. Dzhumagulova, A. N. Jumabekov, and M. K. Dosbolayev, Phys. Plasmas **15**, 053704 (2008).
[19]V. E. Fortov and O. F. Petrov, High Temp. **48**, 943 (2010).
[20]An alternative configuration of illuminating a larger three-dimensional volume and relying on the limited depth-of-focus of the camera might also lend itself to the methods that we test, by using a measurement other than the brightness of the particle. However, we have not developed or tested our method for this case.
[21]M. Zuzic, A. V. Ivlev, J. Goree, G. E. Morfill, H. M. Thomas, H. Rothermel, U. Konopka, R. Sütterlin, and D. D. Goldbeck, Phys. Rev. Lett. **85**, 4064 (2000).
[22]S. Käding and A. Melzer, Phys. Plasmas **13**, 090701 (2006).
[23]M. Kroll, S. Harms, D. Block, and A. Piel, Phys. Plasmas **15**, 063703 (2008).
[24]J. Schablinski, M. Kroll, and D. Block, IEEE Trans. Plasma Sci. **41**, 779 (2013).
[25]W. D. Suranga Ruhunusiri, Ph.D. thesis, the University of Iowa, Iowa City, 2014, Fig. 1.2.
[26]Y. Feng, J. Goree, and B. Liu, Rev. Sci. Instrum. **78**, 053704 (2007).
[27]Random errors in the intensity of a pixel were described in Ref. 26. We choose a random intensity from the empirical noise distribution of Ref. 26 that is centered at an average intensity of 5 on a 8-bit scale of 0 – 255.
[28]See supplementary material at http://dx.doi.org/10.1063/1.4914468 for a synthetic image.
[29]M. H. Thoma, H. Höfner, M. Kretschmer, S. Ratynskaia, G. E. Morfill, A. Usachev, A. Zobnin, O. Petrov, and V. Fortov, Microgravity Sci. Technol. **18**, 47 (2006).
[30]M. H. Thoma, S. Mitic, A. Usachev, B. M. Annaratone, M. A. Fink, V. E. Fortov, H. Höfner, A. V. Ivlev, B. A. Klumov, U. Konopka, M. Kretschmer, G. E. Morfill, O. F. Petrov, R. Sütterlin, S. Zhdanov, and A. V. Zobnin, IEEE Trans. Plasma Sci. **38**, 857 (2010).
[31]M. A. Fink, M. H. Thoma, and G. E. Morfill, Microgravity Sci. Technol. **23**, 169 (2011).
[32]J. Goree, Y. Feng, and B. Liu, Plasma Phys. Controlled Fusion **55**, 124004 (2013).